Published in final edited form as:
J Nanopart Res. 2013 April 1; 15(4): 1651–. doi:10.1007/s11051-013-1651-0.

The novel albumin–chitosan core–shell nanoparticles for gene delivery: preparation, optimization and cell uptake investigation

Mahdi Karimi,
Department of Nanobiotechnology, Faculty of Biological Sciences, Tarbiat Modares University, Tehran, Iran

Wellman Center for Photomedicine, Massachusetts General Hospital, Boston, MA 02114, USA

Department of Dermatology, Harvard Medical School, Boston, MA 02114, USA

Pinar Avci,
Wellman Center for Photomedicine, Massachusetts General Hospital, Boston, MA 02114, USA

Department of Dermatology, Harvard Medical School, Boston, MA 02114, USA

Rezvan Mobasseri,
Department of Nanobiotechnology, Faculty of Biological Sciences, Tarbiat Modares University, Tehran, Iran

Michael R. Hamblin, and
Wellman Center for Photomedicine, Massachusetts General Hospital, Boston, MA 02114, USA

Department of Dermatology, Harvard Medical School, Boston, MA 02114, USA

Harvard-MIT Division of Health Sciences and Technology, Cambridge, MA 02119, USA

Hossein Naderi-Manesh
Department of Nanobiotechnology, Faculty of Biological Sciences, Tarbiat Modares University, Tehran, Iran

Department of Biophysics, Faculty of Biological Sciences, Tarbiat Modares University, Tehran, Iran naderman@modares.ac.ir

Abstract

Natural polymers and proteins such as chitosan (CS) and albumin (Alb) have recently attracted much attention both in drug delivery and gene delivery. The underlying rationale is their unique properties such as biodegradability, biocompatibility and controlled release. This study aimed to prepare novel albumin–chitosan–DNA (Alb-CS-DNA) core–shell nanoparticles as a plasmid delivery system and find the best conditions for their preparation. Phase separation method and ionic interaction were used for preparation of Alb nanoparticles and Alb-CS-DNA core–shell nanoparticles, respectively. The effects of three important independent variables (1) CS/Alb mass ratio, (2) the ratios of moles of the amine groups of cationic polymers to those of the phosphate groups of DNA (N/P ratio), and (3) Alb concentration, on the nanoparticle size and loading efficiency of the plasmid were investigated and optimized through Box–Behnken design of response surface methodology (RSM). The optimum conditions were found to be CS/Alb mass ratio = 3, N/P ratio = 8.24 and Alb concentration = 0.1 mg/mL. The most critical factors for the size of nanoparticles and loading efficiency were Alb concentration and N/P ratio. The optimized nanoparticles had an average size of 176 ± 3.4 nm and loading efficiency of 80 ± 3.9 %.

Correspondence to: Hossein Naderi-Manesh.

Cytotoxicity experiments demonstrated that the prepared nanoparticles were not toxic. The high cellular uptake of nanoparticles (~85 %) was shown by flow cytometry and fluorescent microscopy.

Keywords

Albumin; Chitosan; Nanoparticle; Gene delivery; Optimization

Introduction

Attention to gene therapy as a promising therapeutic approach for the curing of intractable diseases such as inherited conditions and cancer is increasing rapidly (Duan et al. 2008; El-Aneed 2004). In addition, gene therapy can be used as an alternative to conventional protein therapy when cells lack a crucial protein, since it does not have some disadvantages of protein therapy such as systemic toxicity, high in vivo clearance rate and high manufacturing cost (Park et al. 2006). The main purposes of gene therapy are: increasing the expression of a needed target protein via use of nucleic acids and decreasing an unwanted target protein production through use of siRNA and oligonucleotides (De Laporte et al. 2006). However, the main obstacle in gene therapy as an effective treatment approach is the issue of gene delivery, which needs to be resolved (El-Aneed 2004; Ren et al. 2010). Currently, viral carriers and non-viral carriers such as peptides, lipids and dendrimeric or polymeric carriers are the two main types of carriers that are utilized in gene delivery (Che et al. 2011; Cryan et al. 2004; Kim et al. 2011b; Bansal et al. 2010). Although viral delivery has a high efficiency, its broad use is limited by some disadvantages such as high immunogenicity, limitation in terms of size of genetic materials delivered and lack of targeting interaction with certain cells (Duan et al. 2008; El-Aneed 2004; Lee et al. 2011).

One of the most significant non-viral gene delivery systems is the use of cationic polymers, which have positively charged groups in their backbone, which makes it possible to interact with the negative charge of anionic polymers and genetic materials such as plasmids and siRNA. CS is among the most significant cationic polymers that recently have drawn attention for drug and gene delivery (Mao et al. 2010; Lee et al. 2006).

CS is prepared by the partial N-deacetylation of chitin and is composed of α (1-4)-2-amino-2-deoxy β-D-glucan monomers. It is one of the most abundant modified natural polysaccharides that are commonly found in crustacean shells, yeast and fungi (Nagpal et al. 2010). CS is considered as one of the most promising candidates for gene delivery due to its desirable properties such as being biocompatible, biodegradable, non-toxic and inexpensive (Mao et al. 2001; Mansouri et al. 2006; Kim et al. 2011a). Many reports are already in the literature regarding gene delivery and drug delivery to cancer cells using CS nanoparticles (Arya et al. 2011; Kim et al. 2006; Howard et al. 2006). It is able to form strong electrostatic interaction with negatively charged genetic materials via its own cationic amino groups, which is necessary for protection of nuclease degradation (Mao et al. 2010). In summary, due to its particular biopharmaceutical characteristics, CS seems to be among the most suitable carriers in controlled released systems, protein delivery and gene delivery.

Protein-based nanoparticles have attracted considerable attention owing to their advantages such as being non-antigenic, non-toxic, having greater stability and the ability to be scaled up during manufacture (Langer et al. 2003; Rubino et al. 1993; Kommareddy and Amiji 2005; Azarmi et al. 2006). Albumin (Alb), a versatile protein carrier for gene delivery and drug delivery, has some ideal properties for fabrication of nanoparticles such as being non-immunogenic, nontoxic, biodegradable and biocompatible (Kratz et al. 1997; Elzoghby et al.

2012). The presence of different drug binding sites in the Alb molecule makes it possible that high amounts of drugs can be incorporated into the Alb nanoparticle matrix (Patil 2003). Due to the existence of charged amino acids such as lysine and glutamate in the Alb primary structure, the electrostatic adsorption of positively and negatively charged molecules could also be possible (Irache et al. 2005; Weber et al. 2000a). Alb is a soluble and acidic protein that is stable in wide range of pH (4–9), also stable at 60 °C for 10 h and soluble in 40 % ethanol. Its preferential accumulation in solid tumor and inflamed tissues and the above-mentioned properties make it an ideal carrier candidate for gene and drug delivery (Kratz 2008).

Several studies have reported preparation of nanoparticles of Alb with positively charged materials such as poly-L-lysine (PLL), protamine free base and poly(ethyleneglycol)-modified polyethylenimine (Singh et al. 2010; Mayer et al. 2005; Zhang et al. 2010). But, to our knowledge, so far nanoparticles with Alb core and CS shell have not been reported yet. The CS-Alb core–shell nanoparticles are very suitable carriers for delivery of genetic materials and drugs or co-delivery of both of them. Various drugs can be loaded in the core of this type of nanoparticles; moreover, genetic materials can be incorporated in their shells, since DNA can interact with CS via electrostatic interactions. It was shown that nanomorphology could provide significant change in the properties of semiconductors (Xu et al. 2011; Shao et al. 2012; Banerjee and Krupanidhi 2010), but here the main purpose of core–shell structure is to provide two different parts (core, shell) for loading different drugs and nucleic acids and further stabilizing of protein core.

In the present study, the effects of three key factors (CS/Alb mass ratio, N/P ratio and Alb concentration) on the loading efficiency and size of Alb-CS-DNA nanoparticles containing genetic material were assessed by response surface methodology. Finally, cellular uptake and toxicity of the optimized nanoparticles were investigated on the HeLa cell line, which is the oldest, most widely distributed and permanent human cancer cell line (Rahbari et al. 2009).

Materials and methods

Materials

Chitosan (CS) (“low MW”: Cat. No. 448869, Sigma Aldrich) was used after further purification as will be described in “Purification of chitosan” Section BSA (fraction V), glutaraldehyde and all other reagents were purchased from Merck (Germany); they were of analytical grade and used as received. The plasmid psiRNA-hH1GFPzeo was purchased from Invivogen (San Diego, USA). The EndoFree Plasmid Mega Kit (Cat #12381) was from Qiagen. FITC-labeled Bcl2 antisense was purchased from Eurofins MWG Operon (Huntsville, AL). HeLa cells were from ATCC. Trypsin–EDTA (T4049), Dulbecco's modified Eagle's medium (D6046), Dulbecco's phosphate-buffered saline (D8662) and fetal bovine serum (FBS, F2442) were from Sigma.

Purification of chitosan

CS purification was preformed as described in a previous study, however with some modifications (Nasti et al. 2009). Briefly, 3 g of CS was dissolved in 300 mL of acetic acid solution (2 % w/v) in double-distilled water and stirred overnight. The solution was boiled for 15 min to denature and precipitate any possible protein contaminant, and the resultant mixture was then centrifuged at 4,500 rpm for 10 min, in order to separate any aggregated or denatured protein contaminant. Finally, the supernatant was removed and passed through 0.4-lm-pore-size filters. CS was subsequently precipitated from the aqueous phase by adjusting the pH of the solution to 9 through adding 1 N sodium hydroxide. Following

centrifugation, the precipitate was redispersed in water at pH = 9 and again sedimented by centrifugation twice. The procedure was repeated with double-distilled water until the conductivity and pH values became equal with those of pure water. Finally, the sample was stored at 4 °C after freeze-drying.

Plasmid production

The plasmid psiRNA-hH1GFPzeo (vector for generating shRNA targeting GL3 luciferase for use in RNAi experiments) was used as the DNA component for preparation and optimization of Alb-CS-DNA core–shell nanoparticles. Following amplification in TOP10 chemically competent *Escherichia coli* bacteria, it was purified using the EndoFree Plasmid Mega Kit (Qiagen). The concentration and purity of purified plasmid were determined through UV spectrophotometry by measuring absorbance at 260/280 nm.

Nanoparticle preparation

Albumin nanoparticles—Phase separation technique, a technique previously described by Langer et al. and Weber et al., was used for preparing Alb nanoparticles (Langer et al. 2003; Weber et al. 2000b). Briefly, 1 mg/mL of BSA solution was prepared, and the pH was adjusted to 8.2 with 0.01 M NaOH. The variable amount of BSA stock solution was added to 10 mL deionized water with pH 8.2 and 10 mM NaCl. 10 mL of ethanol was added with constant rate (1 mL/min) using a peristaltic pump under constant stirring (550 rpm) at room temperature. After 10 min to dissolve, 8 % glutaraldehyde solution (1.175 μL/mg BSA) was added to the reaction in order to stabilize the nanoparticles. The cross-linking process was carried out through stirring the reaction overnight. Later on, a primary centrifugation was performed to remove the particles that were bigger than 500 nm. Finally, in order to purify the nanoparticles, secondary centrifugation (30,000*g*) and redispersion in deionized water through ultrasonication were performed two times.

Alb-CS-DNA nanoparticles—Firstly, a suitable amount of DNA (psiRNA-hH1GFPzeo) and chitosan corresponding to desired N/P ratio was mixed for 10 min. In preliminary tests, citrate buffer pH = 5.4, phosphate citrate buffer pH = 5.4, sodium acetate buffer pH = 5.4 and phosphate buffer pH = 5.8 all at 20 mM concentration were used. For optimization process, phosphate buffer was used in order to adjust the pH at 5.8. In addition to this, suitable amount of prepared Alb nanoparticles were stirred at 550 rpm. The mixture of CS and DNA was then added to Alb nanoparticles in a drop-wise manner. After 30 min, after primary centrifugation, big aggregates were pelleted and the supernatant was removed and collected in a new tube. Finally, in order to purify the nanoparticles and remove the free polymers, secondary centrifugation (30,000*g*) and redispersion in deionized water through ultrasonication were performed two times. Figure 1 shows the process of preparing Alb-CS-DNA nanoparticles that were used for later analysis.

Characterization of particles

The size and zeta potential of Alb-CS-DNA particles were characterized through photon correlation spectroscopy (PCS) using Malvern Zetasizer ZS series and Scattering Particle Size Analyzer (Malvern Co., UK). The every run of RSM was measured three times, and the value was reported as mean ± standard deviation.

Analytical SEM studies of morphological features were performed for evaluation of shape, size and aggregation of the nanoparticles. To this end, nanoparticle samples were mounted on metal subs which were gold-coated under vacuum, and then examined on a FE-SEM (JSM-6700F; JEOL Ltd., Tokyo, Japan).

FTIR spectra of freeze-dried optimized Alb-CS-DNA nanoparticles, Alb nanoparticles and purified CS were measured using Nicolet IR100 FT-IR Spectrometer. The samples were mixed with pure KBr as the background and compressed into disks using a manual tablet press.

Loading efficiency and loading capacity

To determine the loading efficiency and loading capacity, Alb-CS-DNA nanoparticles with different N/P ratios were centrifuged at 60,000*g* and 15 °C for 60 min and the amount of free plasmid was determined in supernatant by Nanodrop 2000c spectrophotometer (Nano-drop Technologies, Wilmington, DE) at 260 nm using supernatant of non-loaded nanoparticles as basic correction. The amount of incorporated plasmid was calculated by the difference between the initial total amount of plasmid and the measured amount in the supernatant. The every run of RSM was measured three times and the value was reported as mean ± standard deviation. The loading efficiency and loading capacity of nanoparticles were determined by using the following equations:

$$\text{Loading capacity} \quad (\text{LC}\%) = \frac{T_{\text{plasmid}} - F_{\text{plasmid}}}{T_{\text{nanoparticle}}} \times 100 \quad (1)$$

$$\text{Loading efficiency} \quad (\text{LE}\%) = \frac{T_{\text{plasmid}} - F_{\text{plasmid}}}{T_{\text{plasmid}}} \times 100 \quad (2)$$

where T_{plasmid}, F_{plasmid} and $T_{\text{nanoparticle}}$ stand for total amount of plasmid, free amount of plasmid and total amount of nanoparticle, respectively.

Experimental design

Response surface methodology (Box–Behnken experimental design) was selected to optimize the formulation parameters in preparation of Alb-CS-DNA nanoparticles for maximum loading efficiency and minimum diameter. In this study, a 3-factor, 3-level Box–Behnken experimental design was used to optimize the preparation of nanoparticles with independent factors such as CS/Alb mass ratio (X_1), N/P ratio (X2) and Alb concentration (X3) and the three levels as described in Table 1. Range of independent factors has been established by previous studies for development of CS nanoparticles containing genetic materials and preliminary experiments (Lavertu et al. 2006).

The Design Expert (STAT-EASE, 7.0.0, Minneapolis, MN) software was used for generation and evaluation of the statistical experimental design. The design matrix was constructed which included 15 experimental runs. The value of the independent variables and dependent variables are presented in Table 2. For regression analysis of the obtained data as well as estimation of the coefficients in the regression equation, a statistical program in Design Expert 7.0.0 software was used. The equations were validated by ANOVA statistical test. In order to determine the individual and interactive effects of test variables on the responses, response surfaces were plotted. Additional confirmation experiments were then performed so as to verify the validity of the statistical experimental design.

Cytotoxicity of prepared nanoparticles

To investigate the cytotoxicity of prepared nanoparticles, the MTT (3-(4,5-dimethylthiazol-2-yl)-2,5-diphenyltetrazolium bromide) assay was used. Mitochondrial dehydrogenases of viable cells are able to cleave the tetrazolium ring of MTT and produce purple formazan, which is soluble in organic solvent such as dimethylsulfoxide (DMSO) and insoluble in water. For performing the MTT assay, HeLa cells were seeded in each 96-well

plate at a density of 1×10^5 cells/mL in 150 μL of DMEM containing 10 % fetal bovine serum, 100 U/mL penicillin and 100 μg/mL streptomycin at 37 °C in humidified air containing 5 % CO_2. After overnight incubation, the medium was replaced with refreshed medium without FBS and different concentrations of prepared nanoparticles (5–100 μg/mL of nanoparticles) were added. Control well was without nanoparticles. To provide statistically reliable results, all specimens as well as the control were placed in five wells. After 24 h of incubation of cells with different concentrations of nanoparticles, cells were washed with PBS and 100 μL MTT solution (0.5 mg/mL in medium) was added to each well. Following 3 h of incubation at 37 °C and 5 % CO_2, the MTT solution was removed carefully and the formed formazan crystals were dissolved in DMSO. The absorbance was measured at 550 nm in Microplate Reader (Infinite M200, Tecan, Austria). To determine the relative cell viability, the following equation was used:

$$\text{Cell viability } \% = \frac{Abs \quad test}{Abs \quad Control} \times 100 \quad (3)$$

where Abs test and Abs control stand for the absorbance value obtained for treated cells with nanoparticles and untreated cells, respectively.

Cell uptake of the nanoparticles

Cellular uptake of prepared nanoparticles were investigated the HeLa cell line by using the fluorescent FITC-labeled Bcl-2 antisense embedded in Alb-CS-DNA nanoparticles, and this process was performed in a dark setting. The HeLa cells were seeded at 1.2×10^5 cells per well in glass bottom dish, and after 24 h medium from a glass bottom dish was removed and washed with PBS three times before adding 500 μL of FBS-free RPMI containing Alb-CS-FITC-Bcl2 antisense nanoparticles to each well with final concentration of 400 nM. The cells were incubated for 4 h at 37 °C and 5 % CO_2 at dark. Then, the medium of each well was removed and washed by PBS. Following each treatment, the wells were subsequently evaluated by confocal microscopy (Olympus FV1000-MPE).

For quantitative uptake study, flow cytometry was used. The HeLa cells were seeded at 1.2×10^5 cells per well in 24-well plates. To determine the Alb-CS-DNA uptake, FITC-labeled Bcl-2 antisense was used and the cells were incubated with labeled Alb-CS-DNA nanoparticles with final concentration of 400 nM in serum and antibiotics-free medium for 4 h. Treated and untreated cells were washed three times with phosphate-buffered saline (PBS) and detached by trypsinization. Then, the pellet of cells was dispersed in 500 μL PBS. Finally, green emitting light was measured by FACSCalibur (BD FACSCalibur System) flow cytometry, and results were analyzed with FlowJo (v.7.6.1).

Results and discussion

Nanoparticle preparation

Since pK_a of BSA and CS are around 6.5 and 4.7 (Janes et al. 2001; Ge et al. 1998), CS and Alb have positive and negative charge, respectively, in tested pH (5–6), and furthermore, they can interact with each other through electrostatic interactions. In preliminary tests, 4 buffers were used for adjusting pH in the range of 5–6, since only at this range of pH Alb has negative charge and CS has positive charge. In a previous study, it was shown that buffer salts can interfere with preparation of nanoparticles (Langer et al. 2003). Therefore, it seems necessary that we find best candidate buffer for nanoparticle preparation. For this reason, we tested four different buffers. The sizes of nanoparticles using citrate buffer, phosphate citrate buffer, sodium acetate buffer and phosphate buffer were 576 ± 23, 898 ± 32, 403 ± 20 and 291 ± 15 nm, respectively. Among these phosphate buffers, the one which had smallest most desirable size was chosen for optimization experiments.

In a previous study, it was shown that the pH value of the Alb solution had a critical effect on size of Alb nanoparticles; therefore, pH around 8.2 was selected for preparation of the core part of Alb-CS-DNA nanoparticles. To obtain the smallest and most uniform nanoparticles, based on the previous reports, the rate of adding ethanol to Alb solution was adjusted to 1 mg/min (Langer et al. 2003). The size and zeta potential of Alb nanoparticles were 140 ± 4.1 nm and –15 ± 3.2, respectively. The zeta potential and size of nanoparticles increased from around –15 mV and 140 nm to more than +10 mV and 170 nm, after covering of Alb nanoparticle by CS and formation of core–shell nanostructure. These results are consistent with the previous reports where Alb nanoparticles were coated by cationic polymers such as PLL, PEI and PEG-PEI, and in their reports, increases in size and zeta potential have been also observed with exactly the same trends. The reason for increased size and zeta potential of nanoparticles has been suggested to the point that chitosan covered the albumin nanoparticle through electrostatic interactions, and core–shell nanostructure was formed (Wang et al. 2008; Singh et al. 2010; Zhang et al. 2010; Zhang et al. 2008).

Zeta potential and polydispersity index of nanoparticles

For measuring the polydispersity index (PDI) and the zeta potential of Alb-CS nanoparticles, the zetasizer was used. As shown in Table 3, the PDI and zeta potential of nanoparticles ranged from 0.097 to 0.35 and from +10.4 ± 1.3 to +19.7 ± 1.4 mV, respectively. The most effective factors on PDI of nanoparticle were Alb concentration and N/P ratio, but they had opposite trends when we moved from low to high levels of concentration and N/P ratio, respectively. The best PDI was obtained when the Alb concentration was in the lowest level and N/P ratio in the highest level. The most critical factor on the zeta potential was the N/P ratio.

Nanoparticles optimization

The response surface methodology (RSM) uses a combination of mathematical and statistical techniques to design experiments, build models and evaluate the effects of different parameters. The goal is to optimize a number of independent variables in order to achieve the most desired outcome. The optimization process involves investigating the response of the statistically designed combinations, predicting the coefficients by fitting them into a mathematical model which best fits the experimental conditions, estimating the response of the fitted model and checking the adequacy of the model. Central composite design (CCD) and Box–Behnken design (BBD) are among the most frequently used RSM designs and have been widely used in several experiments (Dong et al. 2009). BBD is a spherical and revolving design, which has been applied in optimization of chemical and physical processes due to its logical basis and excellent performance (Muthukumar et al. 2003; Soto-Cruz et al. 1999).

According to the literature and based on preliminary experimentation, CS/Alb mass ratio, N/P ratio and Alb concentration were selected as the independent variables and the size of nanoparticles and loading efficiency as the dependent variables. Box–Behnken design was employed as an experimental design for the analysis of the interactive effect of these parameters and determination of the best conditions for preparation of Alb-CS-DNA nanoparticles.

As we investigated three important factors, the design matrix required 15 experiments; the corresponding experimental data are given in Table 2. As shown in Table 2, the size and loading efficiency of nanoparticles varied from 176.2 ± 3.8–207.3 ± 2.8 nm and 64.94 ± 2–80.06 ± 3.2 %, respectively. As shown in Fig. 2, Alb-CS-DNA nanoparticles are spherical and smooth in shape.

The predicted models were developed applying multiple regression analysis on the experimental data, and as a result, following Eqs. 1 and 2 were acquired. The statistical significance of quadratic models was studied by using the analysis of variance (ANOVA). Regression sum of squares (R^2) for both models which were developed for size and loading efficiency were statistically significant (Table 4).

The statistical significance of the "size" model was shown by *P* value of the model, and it was less than 0.05. However, *P* value of X_2X_3 in the model was higher than 0.05, and its removal from the equation made the model more significant. Therefore, the following equation was the best equation for prediction of size of Alb-CS-DNA nanoparticles:

$$Y2=+188.37-4.11X_1+3.18X_2+8.80X_3-5.71X_1X_2-3.18X_1X_3+2.42X_1^2+4.77X_2^2-4.66X_3^2 \quad (4)$$

where Y2 represents the size of nanoparticles, and X_1, X_2 and X_3 represent CS/Alb mass ratio, N/P ratio and Alb concentration, respectively. The values of *R*2 and adjusted *R*2 for size prediction model were 0.98 and 0.96, respectively. The value of *R*2 was more significant, and this indicated that the model was able to predict nanoparticle size over a specific region of interest. Moreover, there was a good similarity between *R*2 and adjusted *R*2 which indicated the adequacy of the model to predict the size of nanoparticle by optimization process. The model's F-value and CV were 48.35 and 0.88, respectively. This F value implied that the model was significant, and there was very low chance (0.02 %) that an F value as high as the measured one could occur due to noise. The small value of CV indicated a good precision and reliability of the experiments.

In Fig. 3a at fixed Alb concentration of 0.1(mg/mL), the best particle size was achieved when near to low level of CS/Alb mass ratio and low level of N/P ratio were used. In this graph, the biggest nanoparticles were observed at high level of both CS/Alb mass ratio and N/P ratio. Figure 3b illustrates the effects of CS/Alb mass ratio and Alb concentration on the nanoparticle size when the N/P ratio was fixed at 10. In this condition, the minimum size of nanoparticles was maintained at near to middle level of CS/Alb mass ratio and low level of Alb concentration (0.1 mg/mL). Based on these data, we can conclude that Alb concentration had an important role in the size of the nanoparticles, which might be due to the size of Alb core that formed in these concentrations. In a previous study, the effect of Alb concentration on size of Alb nanoparticles was demonstrated (Langer et al. 2003). However, CS/Alb mass ratio has less effect on size of nanoparticles than Alb concentration. In Fig. 3c at fixed CS/Alb mass ratio at 3, the best results were obtained with Alb concentration of 0.1(mg/mL) and lower N/P ratio. The effect of N/P ratio was more obvious when N/P was equal to or more than 10 and the size of nanoparticles became prominently enlarged. The biggest nanoparticles were obtained at Alb concentration of 0.3 (mg/mL) and N/P ratio of 15.

Loading efficiency is another dependent variable that was investigated. Maximum and minimum amounts of loading efficiency were 80.06 ± 3.2 and 64.94 ± 2 %, respectively. *P* value of the "loading efficiency" model was lower than 0.05, indicating the significance of the model. The equation was acquired for prediction of loading efficiency.

$$Y2=+74.55-2.36X_1-2.54X_2+1.04X_3+0.61X_1X_2+3.73X_1X_3+3.94X_2X_3-0.49X_1^2+0.43X_2^2-1.61X_3^2 \quad (5)$$

where Y2 represents the loading efficiency, and X_1, X_2 and X_3 denote CS/Alb mass ratio, N/P ratio and Alb concentration, respectively. The values of R^2 and adjusted R^2 of the model were 0.9792 and 0.9418, respectively.

As Fig. 3d demonstrates, at all values of CS/Alb mass ratio, the maximum loading efficiency was achieved when N/P ratio of 5 was used. It can also be appreciated from the graph that the global-maximum loading efficiency was achieved when N/P ratio and CS/Alb mass ratio were 3 and 5, respectively. It seems that at N/P ratio of 5, more plasmid molecules can interact with CS and at CS/Alb ratio of 3, and most of CS/plasmid complex can attach to Alb core forming Alb-CS-DNA/plasmid nanoparticles. It was shown that complex formation between CS and DNA, promotes protonation of CS. In addition to this, additional 17 % of total glucosamine units were protonated at pH 5.5, following complex formation between CS and DNA. It may explain the high loading efficiency at N/P = 5 rather than at a higher N/P ratio. The same phenomenon has been observed for the interaction of polycations such as PEI with DNA (Utsuno and Uludag 2010). Another study reported the same results for loading efficiency and maximum loading efficiency was obtained at N/P = 5, although they attributed it to increased effective surface area for binding of DNA due to decreased size of nanoparticles (Gazori et al. 2009). In Fig. 3e, at fixed N/P ratio of 5, the minimum loading efficiency was achieved when the CS/Alb mass ratio = 3 and Alb concentration = 0.1 mg/mL were used. Both of these factors have more effect on loading efficiency, and in case of both factors, through moving from high level to low level, increase in loading efficiency was observed. Figure 3f indicates that maximum loading efficiency was achieved at N/P ratio = 5 and Alb concentration = 0.1 mg/mL, when CS/Alb mass ratio was fixed at 3, while minimum loading efficiency in this fixed CS/Alb mass ratio was obtained at low level of Alb concentration and high level of N/P ratio. However, loading capacity of nanoparticles was not subject of optimization, the obtained results showed that loading capacity was affected mostly by N/P ratio (Table 3) and the highest loading capacity (17.56 ± 0.29 %) was achieved when low level of N/P ratio was used.

Optimization

In this study, the goal of optimization was finding the best conditions that give the maximum loading efficiency and minimum nanoparticle size. The regression equation was used for finding the optimal values of the independent variables. The Design Expert software was used for solving the regression equation. The best acquired conditions were at CS/Alb mass ratio = 3, N/P ratio = 8.24 and Alb concentration = 0.1 mg/mL; at these values, the minimum nanoparticle size (176.6 ± 2) and maximum loading efficiency (80.06 ± 3.2) were achieved. The model was validated by conducting five experiments in previously mentioned optimum conditions. Validation experiments and predicted values for both of the responses by the related equations were consistent with each other, so statistical significance of the model was confirmed by these results. Therefore, the model has adequate precision for the prediction of nanoparticle size and loading efficiency in the chosen space of independent variables (in the domain of levels chosen for the independent variables).

FTIR

The FTIR method was applied to elucidate the incorporation of CS and Alb in nanoparticles. Figure 4 shows the FTIR spectra of CS, Alb nanoparticles and Alb-CS-DNA nanoparticles. The FTIR peaks of Alb at 1,532, 1,642, 2,928 and 3,427 cm^{-1} (curve b) are assigned to amide II (the coupling of bending vibrate of N–H and stretching vibrate of C–N), amide I (mainly C = O stretching vibrations), amide A (mainly—NH stretching vibration) and the stretching vibration of –OH bands, respectively (Huang et al. 2010). The peaks of C–O stretching vibration in chitosan appeared at 1,029 and 1,079 cm^{-1} (curve a). The peaks of CS at 1,581, 1,795 and 3,427 cm^{-1} (curve a) are assigned to amide III, I and symmetric vibration of NH, respectively (De Souza Costa-Junior et al. 2009). Hydrogen bonding between OH of CS and OH of Alb results in shifting of 3,427 cm^{-1} (curve a) to 3,414 cm^{-1}, which is the peak. NH_3^+ peak of CS and Alb appeared at 1,581 and 1,642, respectively, NH_3^+ interaction of CS and BSA made a shift from 1,642 to 1,653, and Alb NH_3^+ peak

became stronger. Our finding is validated by the previously reported research (Xu et al. 2012).

Cytotoxicity studies

MTT assay was used for evaluation of cellular toxicity of Alb-CS-DNA nanoparticle on HeLa cells. The result is shown on Fig. 5. Cell toxicity was not observed at 10 μg/mL concentration of Alb-CS-DNA nanoparticles, which indicates that the cell viability is near 100 % at this concentration. At high concentrations of Alb-CS-DNA nanoparticles, cell viability was around 85 %; however, we should note that these higher concentrations are about ten times more than the necessary concentration of Alb-CS-DNA nanoparticles used on the transfection assays for gene delivery. An interesting observation was that when the cell viability of Alb-CS-DNA nanoparticles was compared with CS, the toxicity of CS was a little more than Alb-CS-DNA nanoparticles, while in case of Alb, the cell viability was more than 100 %. This phenomenon can be explained by a nutrient effect (Fischer et al. 2003). This may suggest that the existence of Alb could promote biocompatibility of Alb-CS-DNA nanoparticles.

These results demonstrate that the prepared Alb-CS-DNA nanoparticles are non-toxic and have good biocompatibility in the selected experimental conditions. In addition, our data are also consistent with the previous studies, which have indicated that Alb nanoparticles and Alb nanoparticles coated with PLL and PEI were non-toxic (Wang et al. 2008).

Investigation of cellular uptake by flow cytometry and confocal microscopy

As Alb-CS-DNA nanoparticles contained the FITC dye, the degree of Alb-CS-DNA nanoparticles uptake was quantified with flow cytometry by determining the green fluorescence emitted from Alb-CS-DNA treated cells. The cells with green fluorescence intensity higher than 10^1 were taken as cells containing Alb-CS-DNA nanoparticles by setting the logarithmic fluorescence intensity of untreated cells between 10^0 and 10^1.

Flow cytometry results demonstrated that more than 85 % of HeLa cells had nanoparticle uptake (Fig. 6); hence, the Alb-CS-DNA nanoparticles seem to have good ability for penetrating the cells. For further investigation about the Alb-CS-DNA nanoparticles uptake, confocal microscopy was used. In Fig. 7, the presence of nanoparticles inside the cells was demonstrated, and the image demonstrates that they tend to collect around the nucleus. According to both flow cytometry and confocal microscopy, we can conclude that Alb-CS-DNA nanoparticles have high levels of uptake by the cells (Figs. 6 and 7).

Conclusion

Plasmid-loaded Alb-CS-DNA core–shell nanoparticles were successfully prepared by ionic interaction between opposite charges. Box–Behnken design was used for investigating the effect of three important independent variables (CS/Alb mass ratio, N/P ratio and Alb concentration) on the two dependent variables, that is, loading efficiency and nanoparticle size for optimization of the plasmid-loaded Alb-CS-DNA core–shell nanoparticle. Under the optimal conditions for maximizing the loading efficiency and minimizing nanoparticle size (CS/Alb mass ratio = 3, N/P ratio = 8.24 and Alb concentration = 0.1 mg/mL), the loading efficiency and nanoparticle size were 176.2 ± 3.8 nm and 80.06 ± 3.2 %, respectively, and the model validation was performed by the experimental results. Cytotoxicity tests showed that the optimized nanoparticles have little toxicity and good biocompatibility. High cellular uptake of optimized Alb-CS-DNA nanoparticles was demonstrated by ex vivo cellular uptake (~85 %) studies on HeLa cell line. In comparison with other nanoparticles, this core–shell nanoparticle provides two separate parts for delivery of different drugs and nucleic

acids, and in comparison with PLL and PEI, chitosan is more biocompatible and less toxic, which in turn suggests that core–shell nanoparticle (Alb as a core and CS as a shell) would be more biocompatible. Based on the results of our study, we have concluded that the novel Alb-CS-DNA core–shell nanoparticles can be considered as a potential carrier for gene and drug delivery.

Acknowledgments

This work was partially supported by nano initiative and Tarbiat Modares University. MR Hamblin was supported by US NIH grant R01A1050875.

References

Arya G, Vandana M, Acharya S, Sahoo SK. Enhanced antiproliferative activity of Herceptin (HER2)-conjugated gemcitabine-loaded chitosan nanoparticle in pancreatic cancer therapy. Nanomedicine: Nanotechnology. Biology and Medicine. 2011; 7(6):859–870.

Azarmi S, Tao X, Chen H, Wang Z, Finlay WH, Löbenberg R, Roa WH. Formulation and cytotoxicity of doxorubicin nanoparticles carried by dry powder aerosol particles. Int J Pharm. 2006; 319(1–2): 155–161. [PubMed: 16713150]

Banerjee N, Krupanidhi SB. Facile hydrothermal synthesis and observation of bubbled growth mechanism in nano-ribbons aggregated microspherical Covellite blue-phosphor. Dalton Trans. 2010; 39(41):9789–9793. [PubMed: 20830395]

Bansal KK, Kakde D, Gupta U, Jain NK. Development and characterization of triazine based dendrimers for delivery of antitumor agent. J Nanosci Nanotechnol. 2010; 10(12):8395–8404. [PubMed: 21121345]

Che H-L, Muthiah M, Ahn Y, Son S, Kim WJ, Seonwoo H, Chung JH, Cho C-S, Park I-K. Biodegradable particulate delivery of vascular endothelial growth factor plasmid from polycaprolactone/polyethylenimine electrospun nanofibers for the treatment of myocardial infarction. J Nanosci Nanotechnol. 2011; 11(8):7073–7077. [PubMed: 22103127]

Cryan SA, Holohan A, Donohue R, Darcy R, O'Driscoll CM. Cell transfection with polycationic cyclodextrin vectors. Eur J Pharm Sci. 2004; 21(5):625–633. [PubMed: 15066663]

De Laporte L, Cruz Rea J, Shea LD. Design of modular non-viral gene therapy vectors. Biomaterials. 2006; 27(7):947–954. [PubMed: 16243391]

De Souza Costa-Junior E, Pereira MM, Mansur HS. Properties and biocompatibility of chitosan films modified by blending with PVA and chemically crosslinked. J Mater Sci Mater Med. 2009; 20(2): 553–561. [PubMed: 18987949]

Dong CH, Xie XQ, Wang XL, Zhan Y, Yao YJ. Application of Box-Behnken design in optimisation for polysaccharides extraction from cultured mycelium of Cordyceps sinensis. Food Bioprod Process. 2009; 87(2):139–144.

Duan Y, Zheng J, Han S, Wu Y, Wang Y, Li D, Kong D, Yu Y. A tumor targeted gene vector modified with G250 monoclonal antibody for gene therapy. J Control Release. 2008; 127(2):173–179. [PubMed: 18316136]

El-Aneed A. An overview of current delivery systems in cancer gene therapy. J Control Release. 2004; 94(1):1–14. [PubMed: 14684267]

Elzoghby AO, Samy WM, Elgindy NA. Albumin-based nanoparticles as potential controlled release drug delivery systems. J Controlled Release. 2012; 157(2):168–182.

Fischer D, Li Y, Ahlemeyer B, Krieglstein J, Kissel T. In vitro cytotoxicity testing of polycations: influence of polymer structure on cell viability and hemolysis. Biomaterials. 2003; 24(7):1121–1131. [PubMed: 12527253]

Gazori T, Khoshayand MR, Azizi E, Yazdizade P, Nomani A, Haririan I. Evaluation of Alginate/Chitosan nanoparticles as antisense delivery vector: formulation, optimization and in vitro characterization. Carbohydr Polym. 2009; 77(3):599–606.

Ge S, Kojio K, Takahara A, Kajiyama T. Bovine serum albumin adsorption onto immobilized organotrichlorosilane surface: influence of the phase separation on protein adsorption patterns. J Biomater Sci Polym Ed. 1998; 9(2):131–150. [PubMed: 9493841]

Howard KA, Rahbek UL, Liu X, Damgaard CK, Glud SZ, Andersen MO, Hovgaard MB, Schmitz A, Nyengaard JR, Besenbacher F, Kjems J. RNA interference in vitro and in vivo using a novel chitosan/siRNA nanoparticle system. Mol Ther. 2006; 14(4):476–484. [PubMed: 16829204]

Huang P, Kong Y, Li Z, Gao F, Cui D. Copper selenide nanosnakes: bovine serum albumin-assisted room temperature controllable synthesis and characterization. Nanoscale Res Lett. 2010; 5(6):949–956. [PubMed: 20672034]

Irache JM, Merodio M, Arnedo A, Camapanero MA, Mirshahi M, Espuelas S. Albumin nanoparticles for the intravitreal delivery of anticytomegaloviral drugs. Mini Rev Med Chem. 2005; 5(3):293–305. [PubMed: 15777263]

Janes KA, Fresneau MP, Marazuela A, Fabra A, Alonso MJ. Chitosan nanoparticles as delivery systems for doxorubicin. J Control Release. 2001; 73(2–3):255–267. [PubMed: 11516503]

Kim TH, Jin H, Kim HW, Cho MH, Cho CS. Mannosylated chitosan nanoparticle-based cytokine gene therapy suppressed cancer growth in BALB/c mice bearing CT-26 carcinoma cells. Mol Cancer Ther. 2006; 5(7):1723–1732. [PubMed: 16891458]

Kim J, Lee C-M, Jeong H-J, Lee K-Y. In vivo tumor accumulation of nanoparticles formed by ionic interaction of glycol chitosan and fatty acid ethyl ester. J Nanosci Nanotechnol. 2011a; 11(2): 1160–1166. [PubMed: 21456154]

Kim T-H, Yu GS, Choi H, Shim YJ, Lee M, Choi JS. Preparation of dexamethasone-based cationic liposome and its application to gene delivery in vitro. J Nanosci Nanotechnol. 2011b; 11(2):1799–1802. [PubMed: 21456295]

Kommareddy S, Amiji M. Preparation and evaluation of thiol-modified gelatin nanoparticles for intracellular DNA delivery in response to glutathione. Bioconjug Chem. 2005; 16(6):1423–1432. doi:10.1021/bc050146t. [PubMed: 16287238]

Kratz F. Albumin as a drug carrier: design of prodrugs, drug conjugates and nanoparticles. J Control Release. 2008; 132(3):171–183. [PubMed: 18582981]

Kratz F, Fichtner I, Beyer U, Schumacher P, Roth T, Fiebig HH, Unger C. Antitumour activity of acid labile transferrin and albumin doxorubicin conjugates in in vitro and in vivo human tumour xenograft models. Eur J Cancer. 1997; 33(1008):175.

Langer K, Balthasar S, Vogel V, Dinauer N, von Briesen H, Schubert D. Optimization of the preparation process for human serum albumin (HSA) nanoparticles. Int J Pharm. 2003; 257(1–2): 169–180. [PubMed: 12711172]

Lavertu M, Méthot S, Tran-Khanh N, Buschmann MD. High efficiency gene transfer using chitosan/DNA nanoparticles with specific combinations of molecular weight and degree of deacetylation. Biomaterials. 2006; 27(27):4815–4824. [PubMed: 16725196]

Lee D, Lockey R, Mohapatra S. Folate receptor-mediated cancer cell specific gene delivery using folic acid-conjugated oligochitosans. J Nanosci Nanotechnol. 2006; 6(9–10):2860–2866. [PubMed: 17048492]

Lee K-M, Lee Y-B, Oh I-J. Evaluation of PEG-transferrin-PEI nanocomplex as a gene delivery agent. J Nanosci Nanotechnol. 2011; 11(8):7078–7081. [PubMed: 22103128]

Mansouri S, Cuie Y, Winnik F, Shi Q, Lavigne P, Benderdour M, Beaumont E, Fernandes JC. Characterization of folate-chitosan-DNA nanoparticles for gene therapy. Biomaterials. 2006; 27(9):2060–2065. [PubMed: 16202449]

Mao H-Q, Roy K, Troung-Le VL, Janes KA, Lin KY, Wang Y, August JT, Leong KW. Chitosan-DNA nanoparticles as gene carriers: synthesis, characterization and transfection efficiency. J Controlled Release. 2001; 70(3):399–421.

Mao S, Sun W, Kissel T. Chitosan-based formulations for delivery of DNA and siRNA. Adv Drug Deliv Rev. 2010; 62(1):12–27. [PubMed: 19796660]

Mayer G, Vogel V, Weyermann J, Lochmann D, van den Broek JA, Tziatzios C, Haase W, Wouters D, Schubert US, Zimmer A, Kreuter J, Schubert D. Oligonucleotide-protamine-albumin nanoparticles: protamine sulfate causes drastic size reduction. J Control Release. 2005; 106(1–2): 181–187. [PubMed: 16002173]

Muthukumar M, Mohan D, Rajendran M. Optimization of mix proportions of mineral aggregates using Box Behnken design of experiments. Cement Concr Compos. 2003; 25(7):751–758.

Nagpal K, Singh SK, Mishra DN. Chitosan nanoparticles: a promising system in novel drug delivery. Chem Pharm Bull (Tokyo). 2010; 58(11):1423–1430. [PubMed: 21048331]

Nasti A, Zaki NM, de Leonardis P, Ungphaiboon S, Sansongsak P, Rimoli MG, Tirelli N. Chitosan/TPP and chitosan/TPP-hyaluronic acid nanoparticles: systematic optimisation of the preparative process and preliminary biological evaluation. Pharm Res. 2009; 26(8):1918–1930. [PubMed: 19507009]

Park TG, Jeong JH, Kim SW. Current status of polymeric gene delivery systems. Adv Drug Deliv Rev. 2006; 58(4):467–486. [PubMed: 16781003]

Patil GV. Biopolymer albumin for diagnosis and in drug delivery. Drug Dev Res. 2003; 58(3):219–247.

Rahbari R, Sheahan T, Modes V, Collier P, Macfarlane C, Badge RM. A novel L1 retrotransposon marker for HeLa cell line identification. Biotechniques. 2009; 46(4):277–284. [PubMed: 19450234]

Ren L–L, Wu Y, Han D, Zhao L-D, Sun Q-M, Guo W–W, Sun J-H, Wu N, Li X-Q, Zhai S-Q, Han D-Y, Young W-Y, Yang S-M. Math1 gene transfer based on the delivery system of quaternized chitosan/Na-carboxymethyl–cyclodextrin nanoparticles. J Nanosci Nanotechnol. 2010; 10(11):7262–7265. [PubMed: 21137911]

Rubino OP, Kowalsky R, Swarbrick J. Albumin micro-spheres as a drug delivery system: relation among turbidity ratio, degree of cross-linking, and drug release. Pharm Res. 1993; 10(7):1059–1065. [PubMed: 8378248]

Shao D, Sun H, Yu M, Lian J, Sawyer S. Enhanced ultraviolet emission from poly(vinyl alcohol) ZnO nanoparticles using a SiO2–Au core/shell structure. Nano Lett. 2012; 12(11):5840–5844. [PubMed: 23094803]

Singh HD, Wang G, Uludag H, Unsworth LD. Poly-l-lysine-coated albumin nanoparticles: stability, mechanism for increasing in vitro enzymatic resilience, and siRNA release characteristics. Acta Biomater. 2010; 6(11):4277–4284. [PubMed: 20601248]

Soto-Cruz O, Saucedo-Castañeda G, Pablos-Hach JL, Gutiérrez-Rojas M, Favela-Torres E. Effect of substrate composition on the mycelial growth of Pleurotus ostreatus. An analysis by mixture and response surface methodologies. Process Biochem. 1999; 35(1–2):127–133.

Utsuno K, Uludag H. Thermodynamics of polyethylenimine-DNA binding and DNA condensation. Biophys J. 2010; 99(1):201–207. [PubMed: 20655848]

Wang G, Siggers K, Zhang S, Jiang H, Xu Z, Zernicke RF, Matyas J, Uludag H. Preparation of BMP-2 containing bovine serum albumin (BSA) nanoparticles stabilized by polymer coating. Pharm Res. 2008; 25(12):2896–2909. [PubMed: 18709447]

Weber C, Coester C, Kreuter J, Langer K. Desolvation process and surface characterisation of protein nanoparticles. Int J Pharm. 2000a; 194(1):91–102. [PubMed: 10601688]

Weber C, Kreuter J, Langer K. Desolvation process and surface characteristics of HSA-nanoparticles. Int J Pharm. 2000b; 196(2):197–200. [PubMed: 10699717]

Xu J, Yang X, Wang H, Chen X, Luan C, Xu Z, Lu Z, Roy VAL, Zhang W, Lee C-S. Arrays of ZnO/ZnxCd1–xSe nanocables: band gap engineering and photovoltaic applications. Nano Lett. 2011; 11(10):4138–4143. [PubMed: 21875102]

Xu P, Li W, Zhou H, Pan F, Xing H, Liu H. Investigations of the structural evolution of electrospun nanofibers using atomic force microscopy. RSC Advances. 2012; 2(29):11104–11110.

Zhang S, Wang G, Lin X, Chatzinikolaidou M, Jennissen HP, Laub M, Uludag H. Polyethylenimine-coated albumin nanoparticles for BMP-2 delivery. Biotechnol Prog. 2008; 24(4):945–956. [PubMed: 19194903]

Zhang S, Kucharski C, Doschak MR, Sebald W, Uludag H. Polyethylenimine-PEG coated albumin nanoparticles for BMP-2 delivery. Biomaterials. 2010; 31(5):952–963. [PubMed: 19878992]

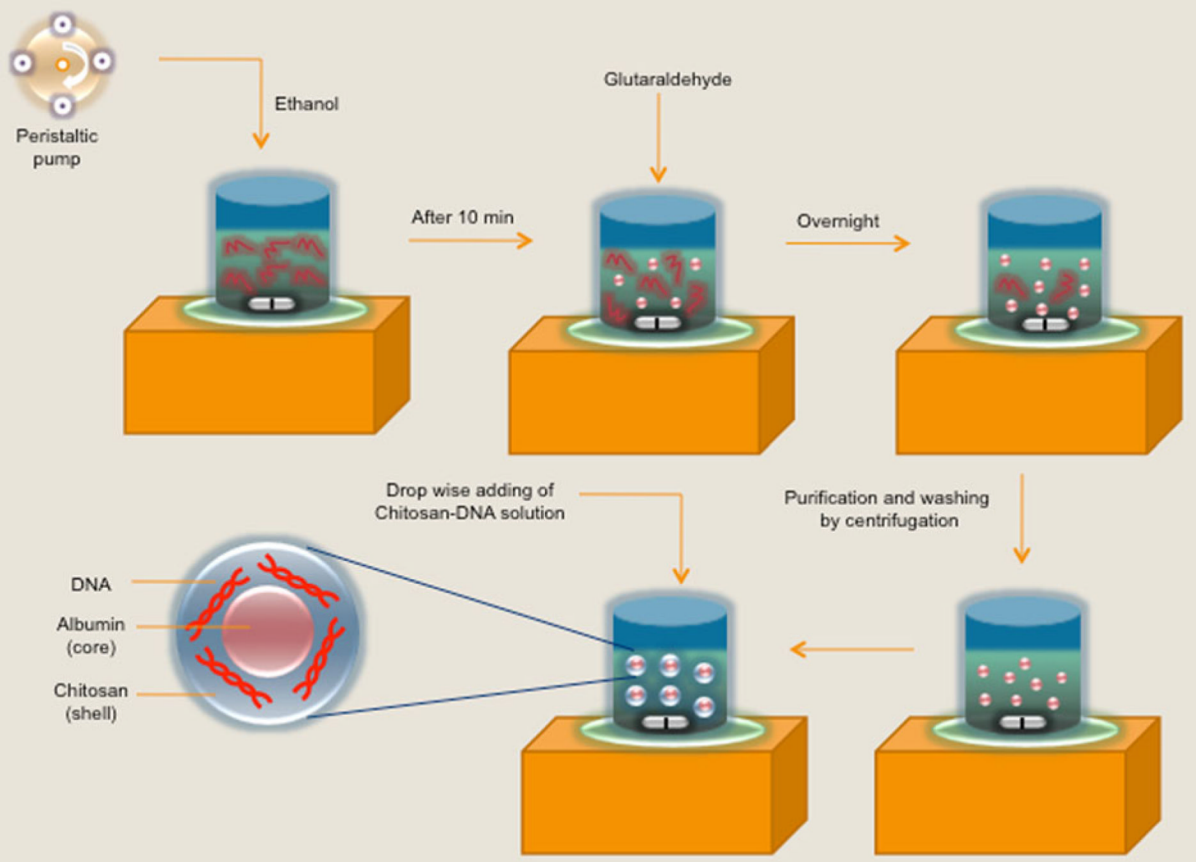

Fig. 1.
Schematic representation of preparation of Alb-CS-DNA nanoparticles

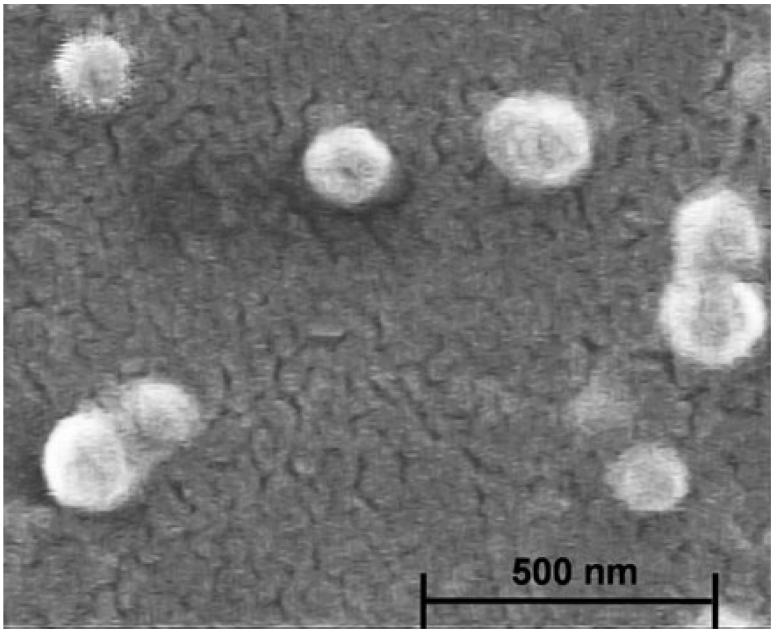

Fig. 2.
SEM image of optimized Alb-CS-DNA nanoparticles

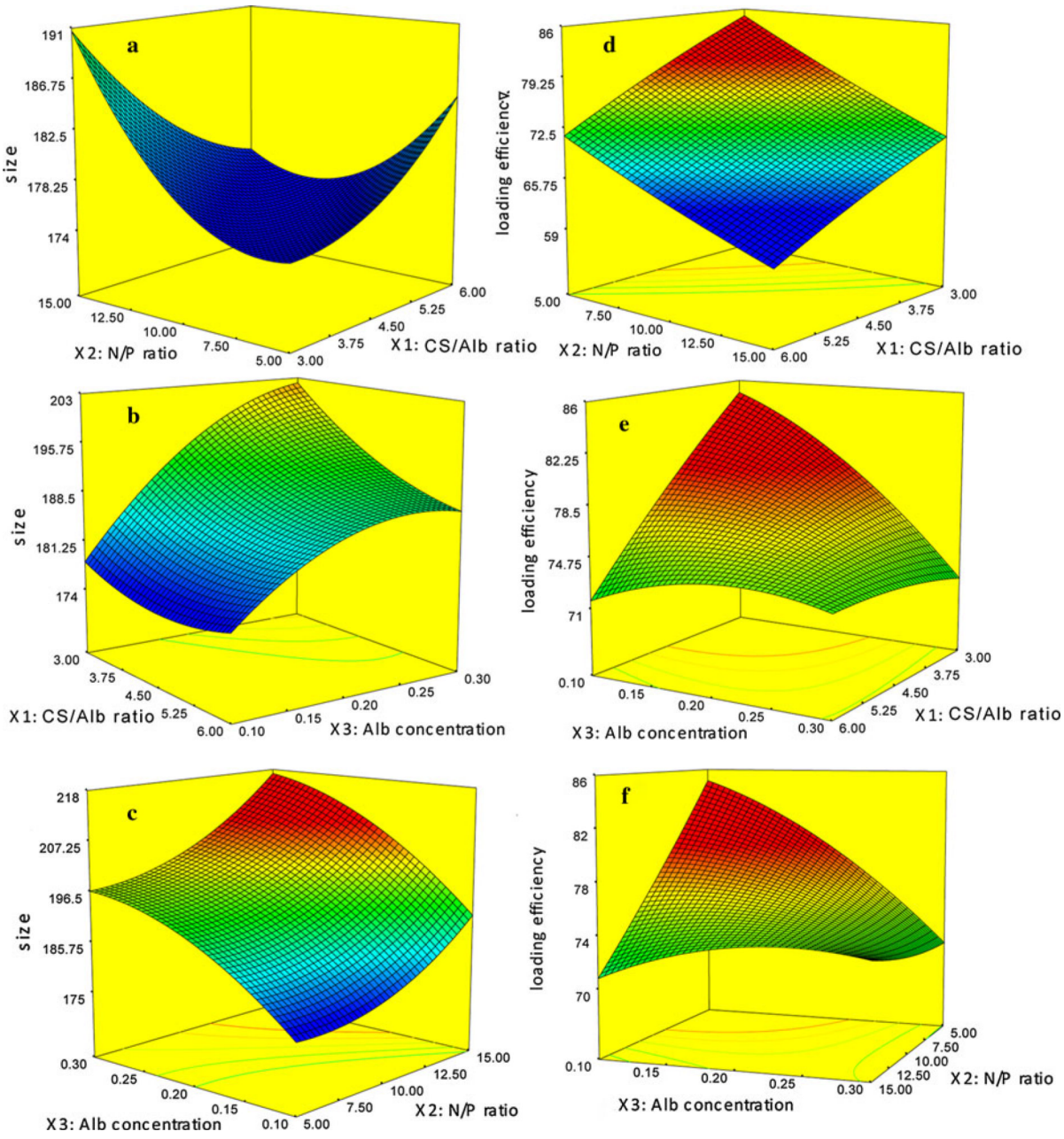

Fig. 3.

Response surface plots (**a**, **b**, **c**, **d**, **e** and **f**) showing the effect of CS/Alb mass ratio, N/P ratio and albumin concentration on the nanoparticles size and loading efficiency

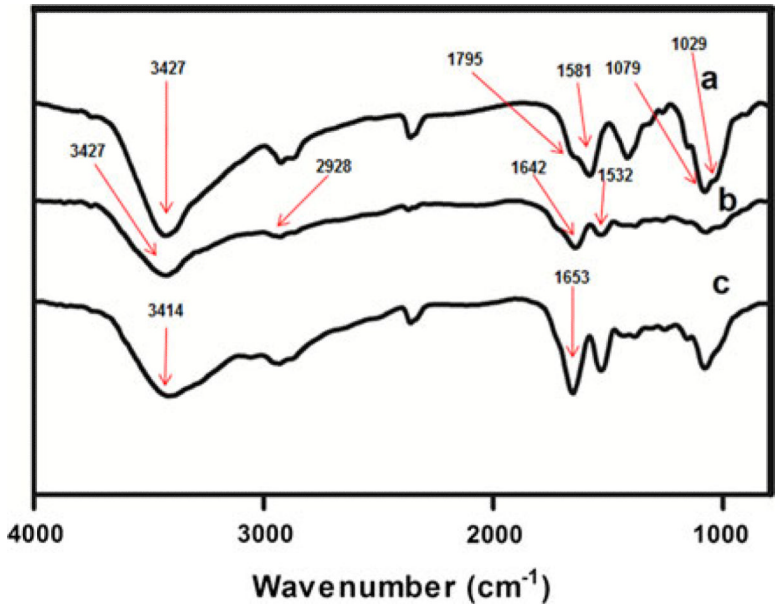

Fig. 4.
FTIR of purified CS (*a*) and Alb nanoparticles (*b*) and Alb-CS-DNA nanoparticles (*c*)

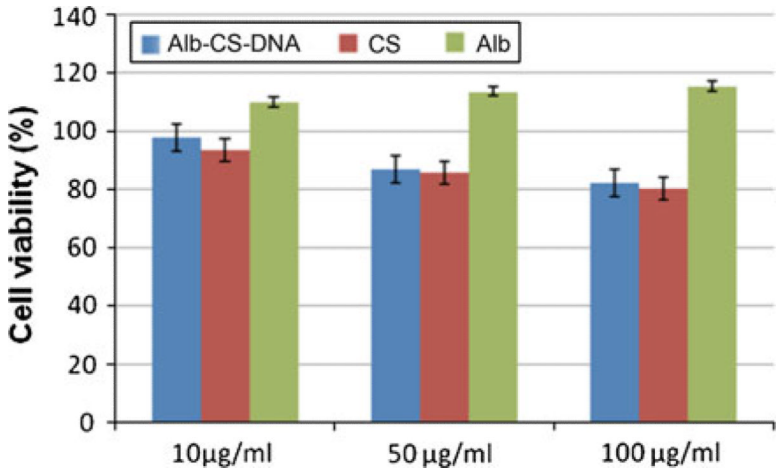

Fig. 5.
MTT assay for different concentrations of the optimized Alb-CS-DNA nanoparticles, CS and Alb

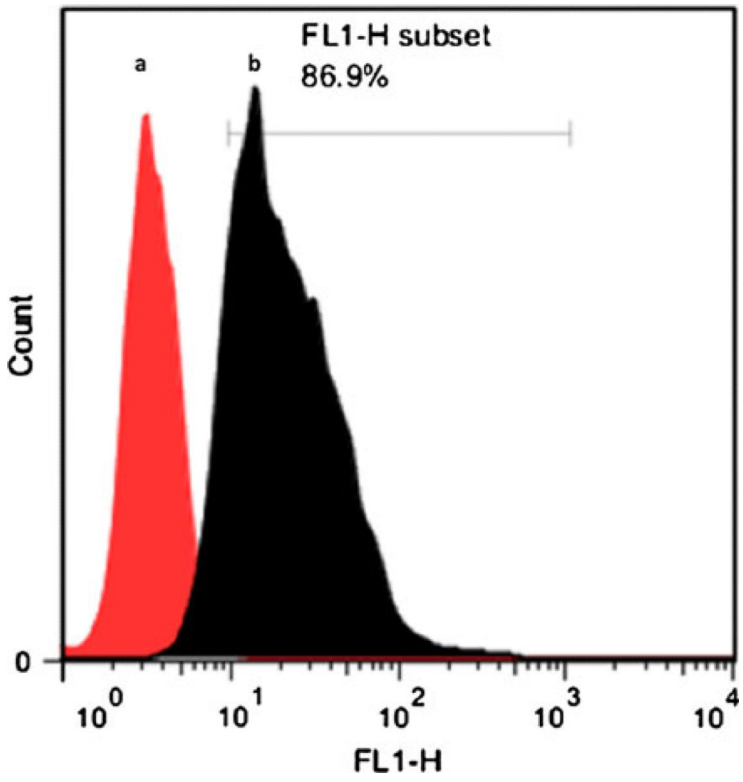

Fig. 6.
Cellular uptake of Alb-CS nanoparticles, HeLa cells treated with nanoparticles for 4 h and the uptake assessed by flow cytometry

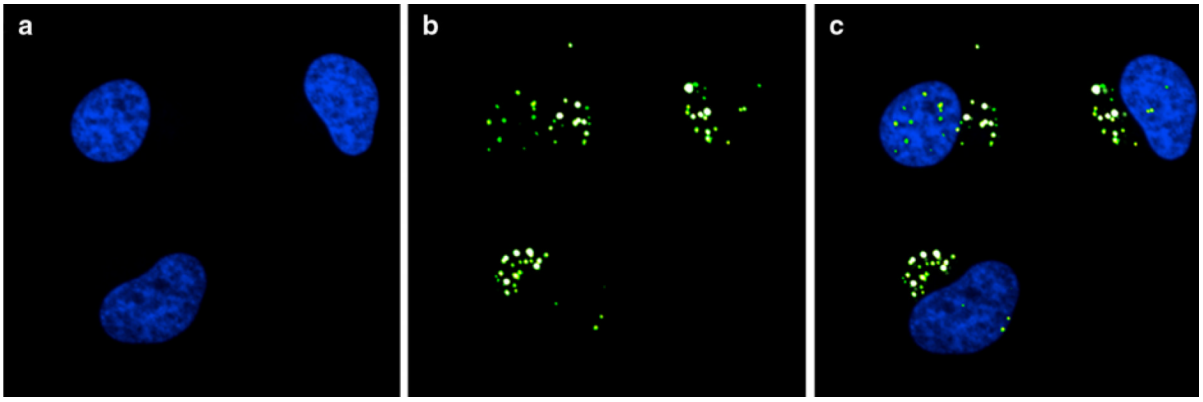

Fig. 7.
Cellular uptake study of FITC-labeled Alb-CS-DNA nanoparticles after 4 h of incubation **a**. Nucleus of cells has been identified through Hoechst staining **b**. Fluorescent image of HeLa cells **c**. (**a**) and (**b**) merged

Table 1

Variables used in central composite experimental design

Independent variables	Symbol	Levels		
		–1	0	1
Chitosan/Albumin ratio	X_1	3	4.5	6
N/P ratio	X_2	5	10	15
Albumin concentration	X_3	0.1	0.2	0.3

Table 2

Box–Behnken design matrix (in coded level of three variables) and response values for nanoparticles size and loading efficiency

Run	Coded variable levels			Independent variables (response)	
	X_1	X_2	X_3	Size (nm)	Loading efficiency (%)
1	–1	–1	0	191.3 ± 1.6	80.06 ± 3.2
2	0	–1	–1	176.2 ± 3.8	79.37 ± 1.6
3	0	0	0	189.9 ± 3.1	75.25 ± 2.7
4	–1	0	–1	179.2 ± 1.7	76.88 ± 1.9
5	0	1	–1	182 ± 2.8	66.31 ± 2.9
6	0	0	0	188 ± 4.4	73.19 ± 3.6
7	–1	0	1	202 ± 1.1	72.5 ± 1.7
8	0	–1	1	192.6 ± 1.7	72.56 ± 2.5
9	0	0	0	187.2 ± 3.3	75.22 ± 2.2
10	0	1	1	203.1 ± 1.7	75.25 ± 1.7
11	1	0	–1	176.6 ± 2	64.94 ± 2
12	1	–1	0	195.23 ± 2.2	73.88 ± 2.9
13	1	0	1	186.7 ± 2.2	75.5 ± 2.5
14	–1	1	0	207.3 ± 2.8	73.88 ± 1.4
15	1	1	0	188.4 ± 3.9	70.14 ± 3

Table 3

Polydispersity index, zeta potential and loading capacity values of prepared CS-Alb-DNA nanoparticles

	X_1	X_2	X_3	PDI	Zeta potential	Loading capacity
1	3	5	0.2	0.163	13.4 ± 1.2	16.75 ± 0.55
2	4.5	5	0.1	0.133	10.4 ± 1.3	17.56 ± 0.29
3	4.5	10	0.2	0.136	15.5 ± 1.3	9.04 ± 0.29
4	3	10	0.1	0.097	17.8 ± 0.9	8.69 ± 0.2
5	4.5	15	0.1	0.089	19.6 ± 1.4	5.6 ± 0.23
6	4.5	10	0.2	0.35	18.8 ± 0.6	8.82 ± 0.39
7	3	10	0.3	0.192	19.1 ± 0.8	8.24 ± 0.17
8	4.5	5	0.3	0.327	14.4 ± 1.1	16.3 ± 0.47
9	4.5	10	0.2	0.14	17.3 ± 1.3	9.04 ± 0.24
10	4.5	15	0.3	0.228	18.6 ± 1.2	6.31 ± 0.13
11	6	10	0.1	0.117	18.5 ± 0.8	8.15 ± 0.23
12	6	5	0.2	0.188	12.2 ± 0.9	17.03 ± 0.55
13	6	10	0.3	0.222	18.1 ± 0.9	9.36 ± 0.28
14	3	15	0.2	0.14	19.7 ± 1.4	5.83 ± 0.1
15	6	15	0.2	0.17	19.5 ± 0.7	6.1 ± 0.24

Table 4

ANOVA results for response surface quadratic model ("size" model)

Variables	Sum of squares	DF	Mean square	*F* value	*p* value Prob > F
Model	1211.51	9	134.61	48.35	0.0002[a]
X_1—chitosan/TPP ratio	135.05	1	135.05	48.51	0.0009[a]
X_2—pH	81.09	1	81.09	29.13	0.0029[a]
X_3—N/P ratio	619.52	1	619.52	222.54	0.0001[a]
$X_1 \times X_2$	130.30	1	130.30	46.81	0.0010[a]
$X_1 \times X_3$	40.32	1	40.32	14.48	0.0126[a]
$X_2 \times X_3$	5.52	1	5.52	1.98	0.2180[b]
X_1^2	21.63	1	21.63	7.77	0.0386[a]
X_2^2	84.03	1	84.03	30.18	0.0027[a]
X_3^2	80.25	1	80.25	28.83	0.0030[a]
Residual	13.92	5	2.78		
Lack of fit	10.07	3	3.36	1.75	0.3844
Pure error	3.85	2	1.92		

[a] Significant ($p < 0.05$)

[b] Not significant ($p > 0.05$)